International Conference on Mathematics, Computational Methods & Reactor Physics (M&C 2009)
Saratoga Springs, New York, May 3-7, 2009, on CD-ROM, American Nuclear Society, LaGrange Park, IL (2009)

QUASI LINEAR REPRESENTATION OF THE ISOTROPIC SCATTERING SOURCE FOR THE METHOD OF CHARACTERISTICS

C. Rabiti and G. Palmiotti
Idaho National Laboratory
2525 North Fremont Avenue, Idaho Falls, ID 83415
cristian.rabiti@inl.gov; Giuseppe.palmiotti@inl.gov

W. S. Yang, M. A. Smith, D. Kaushik, A. B. Wollaber
Argonne National Laboratory
9700 S. Cass Avenue, Argonne, IL 60439
wyang@anl.gov; masmith@anl.gov; kaushik@mcs.anl.gov; awollaber@anl.gov

ABSTRACT

The Method Of Characteristics (MOC) has been widely used for two dimensional lattice calculations. One of the main drawbacks of the MOC is its poor spatial representation of the within-group energy source, which requires the use of a very fine mesh to adequately resolve the neutron flux solution. The most straightforward way to improve the spatial representation of this source would be to project the scalar flux to a set of higher-order trial functions within each mesh element, but this is expensive. An alternative to this has already been proposed that exploits the angular flux moments on the surfaces of each mesh element. In this paper, we present a new alternative in which we define a higher order representation of the isotropic source. The key feature of our method is the introduction of a new, linear discontinuous source representation that does not resort to an expensive spatial projection. This is accomplished by using a P1 approximation to construct the average derivative of the spatial source. So far, the derivation has been done only for a linear representation of the isotropic sources in two and three-dimensional geometries. The paper presents an analysis of the performance of the new method in simple cases and the Takeda 1 benchmarks.

Key Words: Neutron transport, method of characteristics, linear source.

1. INTRODUCTION

The Method of Characteristics (MOC) has been applied extensively in two-dimensional geometries, primarily for lattice calculations. In the framework of the new three-dimensional unstructured mesh code UNÌC [1,2], a Method of Characteristics [3,4] option is under development. One of the main drawbacks of the MOC is its poor spatial representation of the within-group energy source, which requires the use of a very fine mesh to adequately resolve the neutron flux solution. An alternative method for introducing a linear representation of the source, based on the computation of the surface value of the flux moments, has recently been presented [5]. In this paper, we present a new alternative in which we define a higher order spatial representation of the isotropic source. The linear model is built on the knowledge of the space-average value of the source and its derivative. The key feature is the introduction of a new, linear discontinuous source representation that does not resort to an expensive spatial projection. This

is accomplished by using a P1 approximation to construct the average derivative of the spatial source. So far the derivation has been done only for a linear representation of the angular isotropic sources in two- and three-dimensional geometry. We also analyze the performance of the present also the results of the application of this method for a few simple cases and the Takeda 1 benchmark [6].

2. THE METHOD OF CHARACTERISTICS

MOC is widely used for reactor lattice analysis and is well documented; therefore, we will only recall the main aspects of the method. The spatial domain is decomposed in homogenous regions or cell V_i. A set of discrete directions $\vec{\Omega}_n$, $n=1,...,N$ is chosen in order to represent the angular dependence. For each direction a set of parallel lines t_n, termed trajectories or characteristics, are chosen to sample the spatial domain. Along each trajectory the incoming and outgoing fluxes of a region V_i are related by the following equation (isotropic scattering and source assumed):

$$\psi^{out}_{t_n,i} = \psi^{in}_{t_n,i} e^{-R_{t_n,i}\Sigma_{T,i}} + e^{-R_{t_n,i}\Sigma_{T,i}} \int_0^{R_{t_n,i}} dl \left[S(\ell) + \Sigma_{s,i}\phi(\ell) \right] e^{\ell\Sigma_{T,i}} \ . \tag{2.1}$$

If the scalar flux $\phi(\ell)$ and the source $S(\ell)$ are assumed to be constant within each cell, then we can pose $\left[S(\ell) + \Sigma_{s,i}\phi(\ell) \right] = S_i + \Sigma_{s,i}\phi_i = Q_i$ and obtain:

$$\psi^{out}_{t_n,i} = \psi^{in}_{t_n,i} e^{-R_{t_n,i}\Sigma_{T,i}} + Q_i \frac{1 - e^{-R_{t_n,i}\Sigma_{T,i}}}{\Sigma_{T,i}} . \tag{2.2}$$

Eq. (2.2) is not directly solvable since the scalar flux, subsumed in the definition of the source Q_i, depends on the unknown angular flux. Nevertheless Eq. (2.2) is used in an iterative scheme. For the first iteration, the scalar flux (and boundary flux, if reflective boundary conditions are present) is guessed. Eq. (2.2) is then used to propagate the solution along a trajectory through the domain. The value of the scalar flux for the next iteration is provided by the numerical evaluation of the following integral:

$$\langle \phi \rangle_i = \frac{1}{V_i} \int_{V_i} dr \frac{1}{4\pi} \int_{4\pi} d\vec{\Omega}\, \psi(\vec{r}, \vec{\Omega}) \approx \frac{1}{V_i} \frac{1}{4\pi} \sum_{4\pi} \omega_n \sum_{t_n \cap V_i} \omega_\perp \int_0^{R_{t,i}} d\ell\, \psi_{t_n,i}(\ell) \ , \tag{2.3}$$

where ω_n and $\omega_\perp$ are the angular and surface weights of the quadrature formulas. Formulating a balance equation along the trajectory, we get the following expression:

$$\langle \phi \rangle_i \approx \frac{1}{\Sigma_{T,i} V_i} \frac{1}{4\pi} \sum_{4\pi} \omega_n \sum_{t_n \cap V_i} \omega_\perp \left(\psi^{in}_{t_n,i} - \psi^{out}_{t_n,i} + Q_i R_{t_n,i} \right) \ . \tag{2.4}$$

Eqs. (2.2) and (2.4) are iterated upon until convergence is achieved on Q_i.

3. THE QUASI LINEAR REPRESENTATION OF THE SOURCE

We begin by performing a Taylor expansion of the scalar flux along a trajectory (t_n) around the middle point of the intersection length within the element V_i (for simplicity, we drop the indexes t_n and i where it is clear):

$$\phi(\ell) \approx \phi\big|_{\frac{R}{2}} + \frac{\partial\phi}{\partial\ell}\Big|_{\frac{R}{2}} \left(\ell - \frac{R}{2}\right). \tag{3.1}$$

Because

$$\frac{\partial\phi}{\partial\ell} = \vec{\Omega}\cdot\vec{\nabla}\phi, \tag{3.2}$$

Eq. (3.1) can be written as:

$$\phi(\ell) \approx \phi\big|_{\frac{R}{2}} + \vec{\Omega}\cdot\vec{\nabla}\phi\big|_{\frac{R}{2}} \left(\ell - \frac{R}{2}\right). \tag{3.3}$$

In a classical linear interpolation scheme, the within-cell flux can be represented by:

$$\phi \approx \phi\big|_{\vec{r}_g} + \vec{\nabla}\phi\big|_{\vec{r}_g}\cdot\left(\vec{r} - \vec{r}_g\right), \tag{3.4}$$

where $\vec{r}$ is a generic coordinate within the cell and $\vec{r}_g$ is the coordinate of the geometrical centre of the cell. Using this scheme, the spatial averages of the flux and its derivative are related to their evaluated values at the spatial centre by:

$$\begin{aligned}
\langle\phi\rangle &= \frac{1}{V}\int_V d\vec{r}\left(\phi\big|_{\vec{r}_g} + \vec{\nabla}\phi\big|_{\vec{r}_g}\cdot\left(\vec{r} - \vec{r}_g\right)\right) = \phi\big|_{\vec{r}_g} + \frac{1}{V}\vec{\nabla}\phi\big|_{\vec{r}_g}\cdot\int_{V_i} d\vec{r}\left(\vec{r} - \vec{r}_g\right) = \phi\big|_{\vec{r}_g}, \\
\left\langle\vec{\nabla}\phi\right\rangle &= \frac{1}{V}\int_V d\vec{r}\vec{\nabla}\left(\phi\big|_{\vec{r}_g} + \vec{\nabla}\phi\big|_{\vec{r}_g}\cdot\left(\vec{r} - \vec{r}_g\right)\right) = \vec{\nabla}\phi\big|_{\vec{r}_g}.
\end{aligned} \tag{3.5}$$

Therefore, Eq. (3.4) may be written as:

$$\phi \approx \langle\phi\rangle + \left\langle\vec{\nabla}\phi\right\rangle\cdot\left(\vec{r} - \vec{r}_g\right). \tag{3.6}$$

While retaining the first order approximation, we can use Eq. (3.6) to extrapolate the value of the scalar flux and its derivative along the trajectory:

$$\phi(\ell) \approx \langle\phi\rangle + \left\langle\vec{\nabla}\phi\right\rangle\cdot\left(\vec{r}_{t,\frac{R}{2}} - \vec{r}_g\right) + \vec{\Omega}\cdot\left\langle\vec{\nabla}\phi\right\rangle\left(\ell - \frac{R}{2}\right), \tag{3.7}$$

where $\vec{r}_{t,\frac{R}{2}}$ is the coordinate of the middle point of the trajectory.

Now, in order to estimate the average value of the gradient of the flux on the cell, we recall the second equation arising from the projection of the transport equation over the spherical harmonics hierarchy of functions (with isotropic source):

$$\Sigma_{Tot}\vec{J}+\vec{\nabla}\int_{4\pi}d\vec{\Omega}\left(\vec{\Omega}\vec{\Omega}\psi\right)=0\,, \tag{3.8}$$

where $\vec{J}$ is the usual definition of the current. If we assume that the diffusion approximation is acceptable for the representation of the scattering source, then we can write:

$$\Sigma_{Tot}\vec{J}+\frac{1}{3}\vec{\nabla}\phi\approx 0\,, \tag{3.9}$$

The last equation averaged over the cell become:

$$\left\langle\vec{\nabla}\phi\right\rangle\approx-\frac{3\Sigma_{Tot}}{V}\int_{V}dV\vec{J}\quad. \tag{3.10}$$

The average value of the current may be computed as it follows:

$$\begin{aligned}
&\frac{1}{V}\int_{V}dV\vec{J}=\frac{1}{V}\int_{V}dV\int_{4\pi}d\vec{\Omega}\left(\vec{\Omega}\psi\right)=\frac{1}{\sqrt{3}V}\int_{V}dV\int_{4\pi}d\vec{\Omega}\begin{pmatrix}A_{1,-1}\\A_{1,1}\\A_{1,0}\end{pmatrix}\psi,\\
&\frac{1}{V}\int_{V}dV\vec{J}=\frac{1}{\sqrt{3}V}\int_{V}dV\begin{pmatrix}\phi_{1,-1}\\\phi_{1,1}\\\phi_{1,0}\end{pmatrix}=\frac{1}{\sqrt{3}V}\begin{pmatrix}\left\langle\phi_{1,-1}\right\rangle_{i}\\\left\langle\phi_{1,1}\right\rangle_{i}\\\left\langle\phi_{1,0}\right\rangle_{i}\end{pmatrix},
\end{aligned} \tag{3.11}$$

where the quantities $A_{l,m}$ are the orthonormal spherical harmonics over the unit sphere with respect to $\frac{1}{4\pi}\int_{4\pi}d\vec{\Omega}$, and $\phi_{l,m}$ are the angular moments of the flux. Using this last relation in combination with Eq. (3.10) , Eq. (3.7) becomes:

$$\begin{aligned}
&\phi(\ell)\approx\langle\phi\rangle-\frac{3\Sigma_{Tot}}{V}\int_{V}dV\vec{J}\cdot\left(\vec{r}_{t,\frac{R}{2}}-\vec{r}_{g}\right)-\vec{\Omega}\cdot\frac{3\Sigma_{Tot}}{V}\int_{V}dV\vec{J}\left(\ell-\frac{R}{2}\right),\\
&\phi(\ell)\approx\langle\phi\rangle-\frac{\sqrt{3}\Sigma_{Tot}}{V}\begin{pmatrix}\left\langle\phi_{1,-1}\right\rangle\\\left\langle\phi_{1,1}\right\rangle\\\left\langle\phi_{1,0}\right\rangle\end{pmatrix}^{T}\cdot\left(\vec{r}_{t,\frac{R}{2}}-\vec{r}_{g}\right)-\frac{\Sigma_{Tot}}{V}\begin{pmatrix}\left\langle\phi_{1,-1}\right\rangle\\\left\langle\phi_{1,1}\right\rangle\\\left\langle\phi_{1,0}\right\rangle\end{pmatrix}^{T}\left(\ell-\frac{R}{2}\right)\cdot\begin{pmatrix}A_{1,-1}\\A_{1,1}\\A_{1,0}\end{pmatrix}.
\end{aligned} \tag{3.12}$$

Next, since the source term S_i contains the external source, fission source, and the within-group scattering source from other energy groups, it can be treated similarly, assuming that the same, linear spatial representation is employed:

$$Q(\ell) = S(\ell) + \Sigma_s \phi(\ell) \approx Q\Big|_{\frac{R}{2}} + \frac{\partial Q}{\partial \ell}\Big|_{\frac{R}{2}} \left(\ell - \frac{R}{2}\right), \tag{3.13}$$

or:

$$Q(\ell) \approx \langle Q \rangle - \frac{\sqrt{3}\Sigma_{Tot}}{V} \begin{pmatrix} \langle Q_{1,-1} \rangle \\ \langle Q_{1,1} \rangle \\ \langle Q_{1,0} \rangle \end{pmatrix}^T \cdot \left(\vec{r}_{t,\frac{R}{2}} - \vec{r}_g \right) - \frac{\Sigma_{Tot}}{V} \begin{pmatrix} \langle Q_{1,-1} \rangle \\ \langle Q_{1,1} \rangle \\ \langle Q_{1,0} \rangle \end{pmatrix}^T \left(\ell - \frac{R}{2}\right) \cdot \begin{pmatrix} A_{1,-1} \\ A_{1,1} \\ A_{1,0} \end{pmatrix}, \tag{3.14}$$

where:

$$\begin{aligned} \langle Q \rangle &= \langle S \rangle + \Sigma_s \langle \phi \rangle, \\ \langle Q_{1,-1} \rangle &= \langle S_{1,-1} \rangle + \Sigma_s \langle \phi_{1,-1} \rangle, \\ \langle Q_{1,1} \rangle &= \langle S_{1,1} \rangle + \Sigma_s \langle \phi_{1,1} \rangle, \\ \langle Q_{1,0} \rangle &= \langle S_{1,0} \rangle + \Sigma_s \langle \phi_{1,0} \rangle. \end{aligned} \tag{3.15}$$

In order to compute the changes in the propagation equation (Eq. (2.2)), for simplicity we insert Eq. (3.13) in (2.1) to obtain:

$$\psi^{out} = \psi^{in} e^{-R\Sigma_{Tot}} + \langle Q \rangle_i \frac{1 - e^{-R\Sigma_{Tot}}}{\Sigma_{Tot}} + \left\langle \frac{\partial S}{\partial \ell} \right\rangle_V \frac{1}{\Sigma_{Tot}} \left(\frac{R}{2}\left(1 + e^{-R\Sigma_{Tot}}\right) - \frac{1 - e^{-R\Sigma_{Tot}}}{\Sigma_{Tot}} \right). \tag{3.16}$$

The last task is to evaluate the effect of the linear source representation to the balance equation that is used to compute the average angular moment of the flux. The projection over the spherical harmonics averaged over the cell volume leads to:

$$\begin{aligned} \langle \phi_{1,l} \rangle &= \frac{1}{\Sigma_{T,i} V_i} \frac{1}{4\pi} \sum_{4\pi} \omega_n A_{1,l}\left(\vec{\Omega}_n\right) \sum_{t_n \cap V_i} \omega_\perp \left(\psi^{in}_{t_n,i} - \psi^{out}_{t_n,i} \right) \qquad l = -1, 0, 1, \\ \langle \phi \rangle &= \frac{1}{\Sigma_{T,i} V_i} \frac{1}{4\pi} \sum_{4\pi} \omega_n \sum_{t_n \cap V_i} \omega_\perp \left(\psi^{in}_{t_n,i} - \psi^{out}_{t_n,i} \right) + \frac{1}{\Sigma_{T,i} V_i} \frac{1}{4\pi} \sum_{4\pi} \omega_n \int_{S_\perp} ds \int_0^R d\ell Q(\ell). \end{aligned} \tag{3.17}$$

Using the expression for the source provided by Eq. (3.13), we find:

$$\int_{S_\perp} ds \int_0^R d\ell Q(\ell) = \int_{S_\perp} ds \int_0^R d\ell \left(Q\big|_{\frac{R}{2}} + \frac{\partial Q}{\partial \ell}\Big|_{\frac{R}{2}} \left(\ell - \frac{R}{2} \right) \right) = \int_{S_\perp} ds \int_0^R d\ell \, Q\big|_{\frac{R}{2}} =$$
$$= \sum_{t_n \cap V_i} \omega_\perp R_{t_n} \left(\langle Q \rangle + \left\langle \vec{\nabla} Q \right\rangle \cdot \left(\vec{r}_{t_n, \frac{R_{t_n}}{2}} - \vec{r}_g \right) \right). \tag{3.18}$$

Substitution of Eq. (3.18) into Eq. (3.17) allows the computation of the average scalar flux.

Since the evaluation of the term $\left\langle \vec{\nabla} \phi \right\rangle \cdot \left(\vec{r}_{t, \frac{R}{2}} - \vec{r}_g \right)$ in Eq. (3.7) involves the storage of the coordinate of the geometrical centre of each cell and the computation 'on the fly' of the coordinate of the middle point of the trajectory, we considered also the option of neglecting this contribution by using the approximation:

$$\phi(\ell) \approx \langle \phi \rangle + \vec{\Omega} \cdot \left\langle \vec{\nabla} \phi \right\rangle \left(\ell - \frac{R}{2} \right) \tag{3.19}$$

In the results section we refer to this as 'scheme 2' in opposition to the more accurate one named 'scheme 1'.

3.1 Order of Accuracy Considerations

Because the method of characteristics is based on a histogram spatial representation of the source term, it is generally bounded to a first order convergence behavior except when there is no scattering or fission in the medium. Using this, it is easy to prove that our new approach does not lead to a higher order convergence behavior. To show this, we define the function f_2

$$\vec{\nabla} f_2 = \vec{\nabla} \int_{4\pi} d\vec{\Omega} \left(\vec{\Omega} \vec{\Omega} \psi \right) - \frac{1}{3} \vec{\nabla} \phi \ , \tag{3.20}$$

and write Eq. (3.10) in the following exact form:

$$\left\langle \vec{\nabla} \phi \right\rangle = -3 \Sigma_{Tot} \left\langle \vec{J} \right\rangle - 3 \left\langle \vec{\nabla} f_2 \right\rangle . \tag{3.21}$$

Using this expression in Eq. (3.7) gives the exact expression of Eq. (3.12):

$$\phi(\ell) = \langle \phi \rangle - 3 \Sigma_{Tot} \left(\left\langle \vec{J} \right\rangle + \left\langle \vec{\nabla} f_2 \right\rangle \right) \cdot \left(\vec{r}_{t, \frac{R}{2}} - \vec{r}_g \right) - 3 \Sigma_{Tot} \vec{\Omega} \cdot \left\langle \vec{J} \right\rangle \left(\ell - \frac{R}{2} \right) \tag{3.22}$$

This exact relation (with respect the angular variable), compared to Eq. (3.12), proves that the error that we commit in the evaluation of the scattering source is still of first order. But instead of being proportional to the gradient of the scalar flux, it is now proportional to the gradient of the second order angular moment of the flux. As the importance of the self scattering source increases, the same will occur for the proportionality coefficient for the linear behavior of the standard MOC error for the treatment of the self scattering source. In the situation just described,

the diffusion behavior will be dominant; therefore, we should aspect larger advantage where the self scattering is a dominant phenomenon.

4. RESULTS

The first test sets are purely theoretical in order to clearly evaluate the asymptotic behavior of the approximation. For the first set of tests, we consider a 2D square of dimensions 25 by 25 cm with one energy group, vacuum boundary condition, 1 polar and 5 azimuthal angles (40 directions on the full sphere), and a constant trajectory spacing of 0.01 cm. Using these settings we have performed K_{eff} calculations using four set of different cross section (see Table I), and we have evaluated the error behavior with respect to a homogeneous refinement of a regular Cartesian mesh.

Table I. Cross section sets

Set	Cross section			
	Total	**Scattering**	**Fission**	**Nu*Fission**
I	1.000	0.050	0.050	0.050
II	1.000	0.500	0.500	0.500
III	0.100	0.050	0.050	0.050
IV	0.01	0.005	0.005	0.005

The four sets of cross sections are chosen to probe different problem typologies. The first set is a problem dominated by the absorptions in a thick media, the second is diffusion dominated, the third represents an intermediate problem, and the fourth is transport dominated via the leakage component.

Figures 1 through 4 show the error on K_{eff} as a function of mesh refinement. The reference case used to compute the "fully-converged" solution of each problem is always 'scheme 1' with a regular mesh spacing of 0.049 cm. Recall that 'scheme 1' and 'scheme 2' are implementations of the quasi linear source with scheme 2 employing a less expensive and less accurate representation of the distance to the cell centre [see Eq. (1.23)].

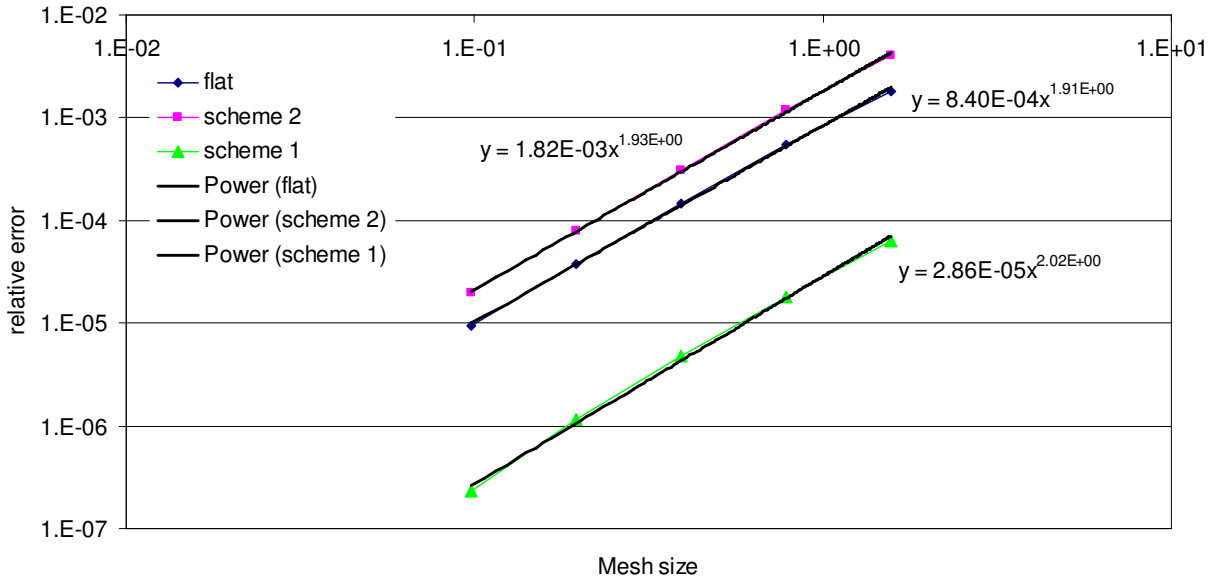

Figure 1: Error Behavior, Cross Section Set I.

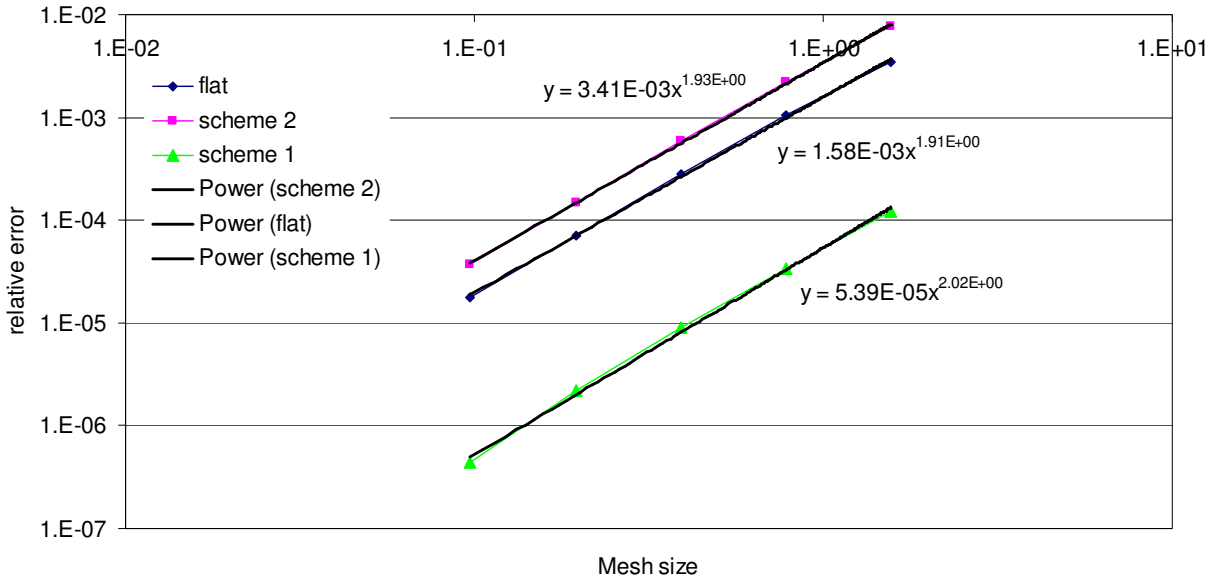

Figure 2: Error Behavior, Cross Section Set II.

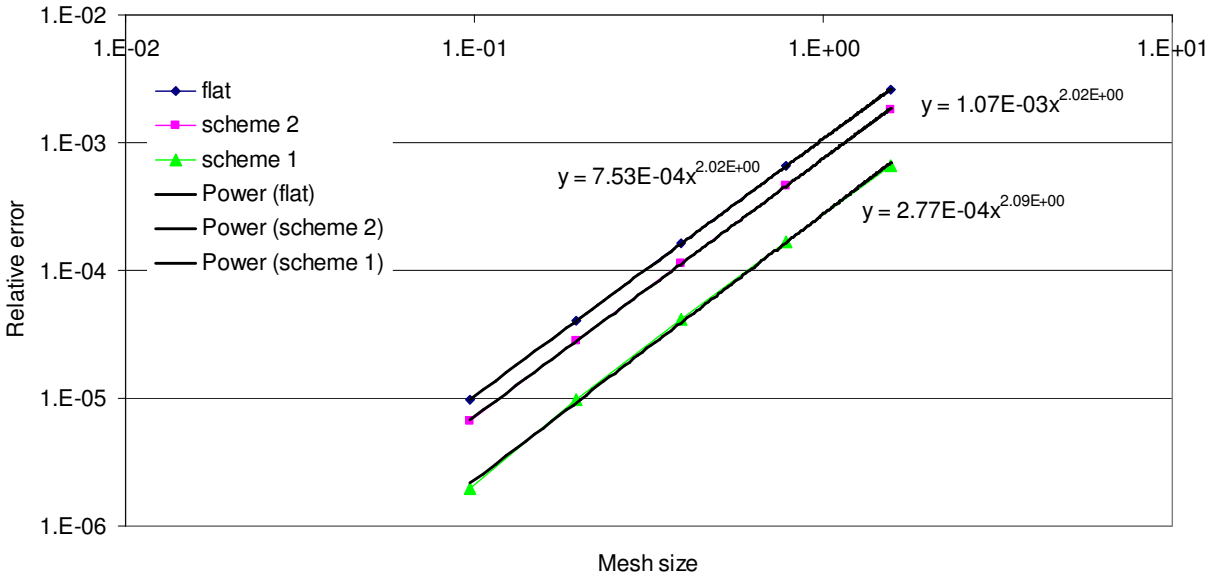

Figure 3: Error Behavior, Cross Section Set III.

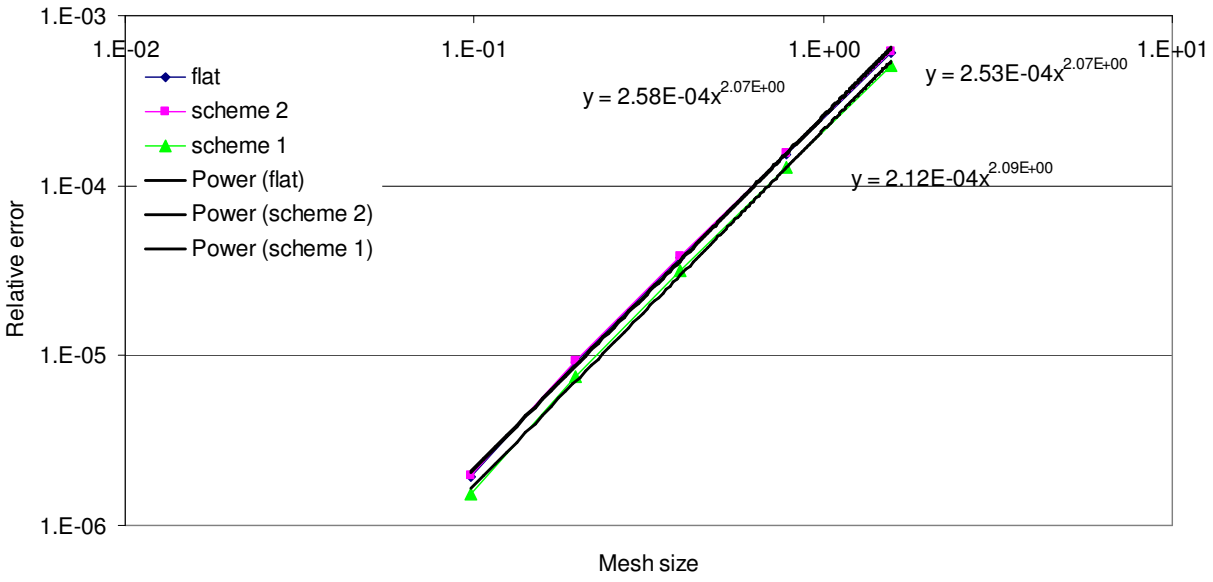

Figure 4: Error Behavior, Cross Section Set IV

For all the methods applied to each problem, the spatial convergence of the eigenvalue is second order (the increasing of one order of accuracy is due to the fact that K_{eff} is an integral measure). This is in agreement with the discontinuous flat source approximation. The error proportionality coefficient is what changes as a function of the composition and method. Both the first and second scheme improve the coefficient, but the first approach has a much higher payback. Two metrics are considered to measure of the performance of the scheme. The first is the minimum

and maximum gain factor with respect to the classical scheme, and the second is the gain over the maximum of the error proportionality coefficient over all problem sets.

Table II. Linear Scheme Performance

Cross section set	Gain factors		Error proportionality coefficient		
	Scheme 1	Scheme 2	Scheme 1	Scheme 2	Flat
I	63	2.1	$2.9\ 10^{-5}$	$8.4\ 10^{-4}$	$1.8\ 10^{-3}$
II	63	2.2	$5.4\ 10^{-5}$	$1.5\ 10^{-3}$	$3.4\ 10^{-3}$
III	3.9	1.5	$2.8\ 10^{-4}$	$7.5\ 10^{-4}$	$1.1\ 10^{-3}$
IV	1.2	1	$2.1\ 10^{-4}$	$2.5\ 10^{-4}$	$2.5\ 10^{-4}$
Maximum	63	2.2	$2.5\ 10^{-4}$	$1.5\ 10^{-3}$	$3.4\ 10^{-3}$
Gain factors over maxima	13.6	1.36			

Table II definitively depicts the superior performance of scheme 1. Moreover, it is important to note that in two cases (see Figs. 1 and 2), the quasi linear source provides more than a factor of ten increase in accuracy. The increase in computational cost relative to traditional MOC for a fixed mesh size was about 21% for scheme 2 and 29% for scheme 1.

As a more realistic application of the method, we simulated the control rod inserted case of the Takeda 1 benchmark [6]. Due to the much better performance of scheme 1, we implemented only it into the 3-D version of the code. For the simulation we used the S_4 angular quadrature formula (48 directions on the full sphere) and a trajectory spacing of 0.01 cm^2. For the three dimensional case, the increase of the computational cost was higher than in the two dimensional tests, reaching 50%. The simulation showed that both the flat and the new scheme in this case were converging at a higher rate than the expected first order (see Figure 5). Due to time and resourece limitations, it was not possible to do further mesh refinement to obtain the complete asymptotic convergence rate. The comparison of the K_{eff} values (see Table III) shows that the two code versions converge to a slightly different K_{eff}, therefore we performed the error convergence analysis of each version with respect to its own solution at 512,000 mesh elements. The discrepancies in the K_{eff} values has yet to be fully explained. So far, we believe that they are connected to differences in the numerical integration of each element via the trajectory intersections. Increasing the trajectory density was not possible due to memory limitations, but in order to confirm our supposition we have observed that Eq. (3.18) may be written as:

$$\int_{S_\perp} ds \int_0^R d\ell Q(\ell) = \int_{S_\perp} ds \int_0^R d\ell \, Q|_{\frac{R}{2}} = \int_{S_\perp} ds \int_0^R d\ell \left(\langle Q \rangle + \langle \vec{\nabla} Q \rangle \cdot \left(\vec{r}_{t,\frac{R}{2}} - \vec{r}_g \right) \right) =$$

$$= V \langle Q \rangle - V \langle \vec{\nabla} Q \rangle \vec{r}_g + \langle \vec{\nabla} Q \rangle \int_{S_\perp} ds \int_0^R d\ell \left(\frac{R}{2}, \vec{s} \right) = \tag{4.1}$$

$$V \langle Q \rangle - V \langle \vec{\nabla} Q \rangle \vec{r}_g + \langle \vec{\nabla} Q \rangle \int_{S_\perp} ds \int_0^R d\ell (l, \vec{s}) = V \langle Q \rangle .$$

We have implemented Eq. (4.1) into the code and refer to it as scheme 3. This is equivalent to assuming that the trajectory-sampled estimate of the cell geometrical centre is equivalent to the analytical cell centre. Of course, this approximation strongly degrades the method performance as the number of trajectories decreases (see Figure 5 and Table III). At present, a renormalization of the trajectory-cell intersection that preserves the location of the cell geometrical center during its numerical computation is under evaluation. At any rate, this approach demonstrates that different approaches in the numerical sampling of the domain can lead to different eigenvalue estimations.

Table III. Takeda 1, K_{eff} Values

Number of mesh cell	Cross section		
	Scheme 1	Flat	Scheme 3
1000	0.95675	0.92948	0.94380
8000	0.96131	0.95698	0.95851
64000	0.96222	0.96216	0.96179
512000	0.96233	0.96253	0.96228

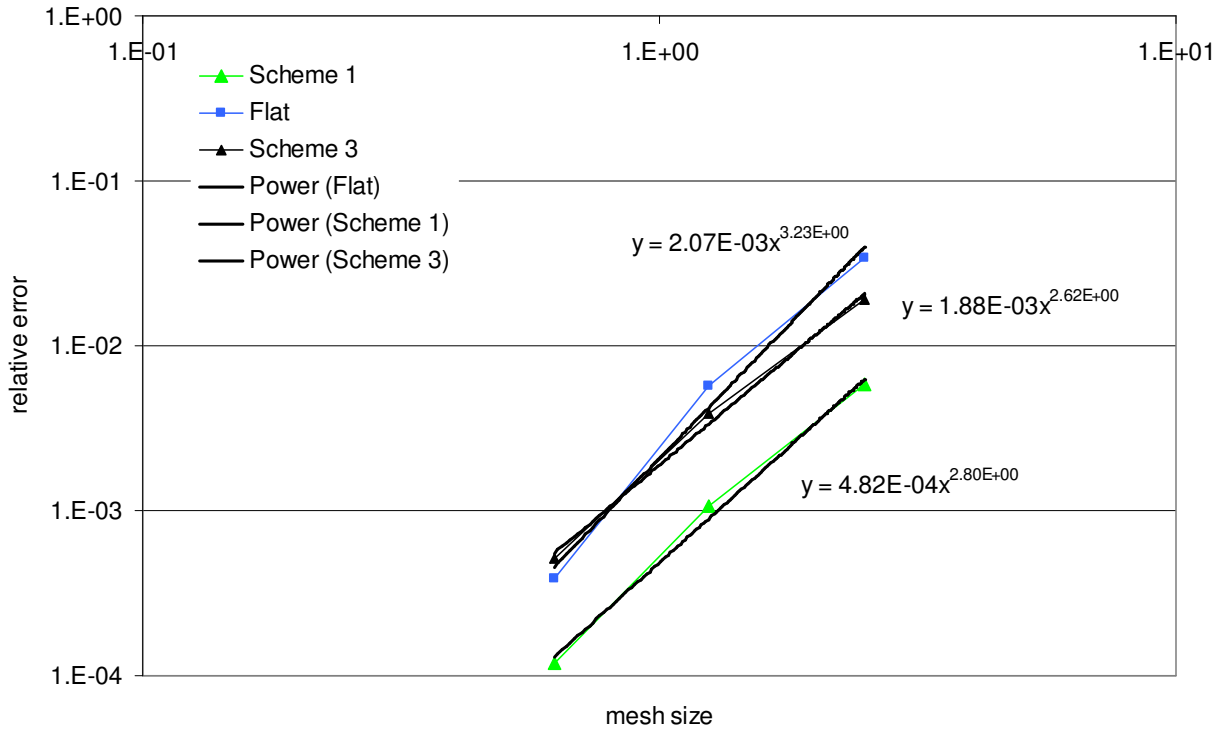

Figure 5: Error Behavior, Takeda 1.

5. CONCLUSION

We have presented a new methodology to compute a quasi linear spatial representation of the within-group energy source in the MOC propagation equation that does not resort to an expensive projection to high order spatial trial functions. This was done by making use of a P_1 approximation to construct the average derivative of the spatial flux. This methodology has relatively low additional computational and memory costs. Results in simple test cases are encouraging; two cases demonstrated over an order of magnitude improvement in eigenvalue accuracy at a computational cost increase of about 20%. Although this methodology is not very effective in transport dominated cases (see Figure 4), for these cases MOC is already competitive with other methods. Unfortunately, the application of our scheme to the Takeda-1 benchmark has exposed some complications that were hidden in the preliminary tests. We believe that these difficulties can be overcome, and it should be possible to translate the gain factor seen in the first tests to realistic problems. The introduction of the linear source representation will hopefully lead to the possibility of enhancing the current Algebraic Collapsing Acceleration [7], at present used in the code, to also include a linear representation of the scalar flux. This last step will improve the consistency and the effectiveness of the acceleration.

ACKNOWLEDGMENTS

This work has been carried out for the U.S. Department of Energy Office of Nuclear Energy Under DOE Idaho Operations Office Contract DE-AC07-05ID14517 (INL/CN-08-14429). This research used resources of the High Performance Computing center at INL.

REFERENCES

1. Palmiotti G., Smith M. A., Rabiti C., Kaushik D., Siegel A., Smith B., and Lewis E. E., "UNÌC: Ultimate Neutronic Investigation Code.", in Proceedings of Joint International Topical Meeting on Mathematics & Computation and Supercomputing in Nuclear Applications (M&C + SNA 2007). Monterey, California.
2. Micheal A. Smith, Chang-Ho Lee, Dinesh Kaushik, Allan Wollaber, and Won Sik Yang, "Report on Fuel Cycle Neutronics Code Development in FY2008," GNEP-REAC-PMO-MI-DV-2008-000177, Sept. 2008.
3. Askew J. R., "A Characteristics Formulation of the Neutron Transport Equation in Complicated Geometries", AAEW-M 1108, United Kingdom Atomic Energy Establishment (1972).
4. Carlson B. G., "A Method of Characteristic and Other Improvements in Solution Methods for the Transport Equation, " Nucl.Sci. Eng., 61, 408, (1976).
5. S. Santandrea, R. Sanchez and P. Mosca, "A Linear Surface Characteristics Scheme for Neutron Transport in Unstructured Meshes", Nucl. Sci. Eng. 160, 23, (2008).
6. Takeda T. and Ikeda H., "3-D Neutron Transport Benchmarks," NEACRP-1-300 OECD/NEA, Organization of Economic Cooperation and Development/Nuclear Energy Agency. 1991.
7. Suslov I. R., "An Algebraic Collapsing Acceleration in Long Characteristics Transport Theory, " Proc. 11th Symp. Atomic Energy Research, Csopak, Hungary (2001).